# Electrochemically Controlled Swelling and Mechanical Properties of a Polymer Nanocomposite

Daniel J. Schmidt,[†] Fevzi Ç. Cebeci,[†,‡] Z. Ilke Kalcioglu,[‡] Samantha G. Wyman,[†] Christine Ortiz,[‡] Krystyn J. Van Vliet,[‡,§,*] and Paula T. Hammond[†,*]

[†]Department of Chemical Engineering, [‡]Department of Materials Science and Engineering, and [§]Department of Biological Engineering, Massachusetts Institute of Technology, Cambridge, Massachusetts 02139

S timuli-responsive polymeric materials have attracted much interest for a variety of applications including drug delivery, biological and chemical sensing, separations, and mechanical actuation, among others.[1−5] Control over the mechanical properties of a surface is of particular interest for the modulation of cellular behavior, as it is well-known that adhesion of cells to surfaces can be modulated *via* the stiffness of those surfaces.[6,7] In the area of biomimicry, researchers have recently designed a chemoresponsive polymer nanocomposite to mimic the dermis of the sea cucumber, a marine organism that can reversibly alter its stiffness.[8] Stimuli-responsive composite materials open up the possibility of tuning percolative behavior, which can dramatically alter mechanical, electrical, optical, and other composite properties.[9,10] In this work, we have designed and characterized an electrochemically responsive polymer nanocomposite thin film with actively tunable mechanical properties. Electrochemical stimuli are advantageous, in comparison with temperature or pH changes, in that they can be applied reversibly, rapidly, and locally (*i.e.*, at an electrode instead of throughout the bulk). Moreover, the structure and function of biological molecules, cells, and organisms, for example, may be inadvertently altered by large changes in temperature or pH, whereas application of a small voltage maintains a comparatively mild environment.

Layer-by-layer (LbL) assembly, introduced by Decher in the 1990s,[11] was employed here for the fabrication of an electroactive thin film composite. LbL assembly is a simple and versatile process that involves the sequential adsorption of oppositely

**ABSTRACT** We present the layer-by-layer assembly of an electroactive polymer nanocomposite thin film containing cationic linear poly(ethyleneimine) (LPEI) and 68 vol % anionic Prussian Blue (PB) nanoparticles, which allow for electrochemical control over film thickness and mechanical properties. Electrochemical reduction of the PB doubles the negative charge on the particles, causing an influx of water and ions from solution to maintain electroneutrality in the film; concomitant swelling and increased elastic compliance of the film result. Reversible swelling upon reduction is on the order of 2−10%, as measured *via* spectroscopic ellipsometry and electrochemical atomic force microscopy. Reversible changes in the Young's elastic modulus of the hydrated composite film upon reduction are on the order of 50% (from 3.40 to 1.75 GPa) as measured with *in situ* nanoindentation, and a qualitative increase in viscous contributions to energy dissipation upon redox is indicated by electrochemical quartz crystal microbalance. Electrochemical stimuli maintain a mild operating environment and can be applied rapidly, reversibly, and locally. We maintain that electrochemical control over the swelling and mechanical behavior of polymer nanocomposites could have important implications for responsive coatings of nanoscale devices, including mechanically tunable surfaces to modulate behavior of adherent cells.

**KEYWORDS:** polymer nanocomposite · electrochemistry · Prussian Blue · responsive materials · layer-by-layer thin film · swelling · nanoindentation

charged materials onto a charged substrate. While the stiffness of LbL films can be controlled by post-assembly cross-linking,[12,13] as well as assembly pH and choice of polymer,[7] these films can also be stimuli-responsive.[14] It is known that changes in humidity[15] and ionic strength[16] can reversibly alter the stiffness of LbL films by changing the degree of film hydration and the degree of ionic cross-linking, respectively. There are only a few examples in the literature of reduction−oxidation (redox)-driven swelling of LbL films. The Calvo group has studied multilayer films containing a ferrocene-derivatized poly-allylamine (PAH-Fc)[17] as well as an osmium complex-derivatized polyallylamine (PAH-Os),[18] which can swell by 10% of initial film thickness upon oxidation of the Os(II). The Vancso group has layered anionic and cationic polyferrocenylsilanes to form multilayer capsules, which expand and increase
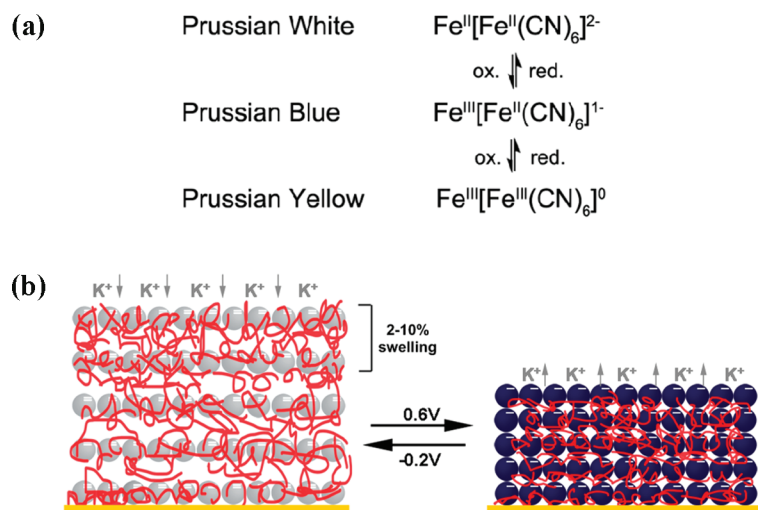
their permeability upon chemical oxidation of the ferrocene units.[19] Most recently, Grieshaber *et al.* reported on a poly(L-glutamic acid)/poly(allylamine hydrochloride) multilayer film that takes up ferrocyanide ions from solution and can expand and contract by 5−10% in response to electrochemical oxidation and reduction of the ferrocyanide species.[20] None of the above reports on redox-driven swelling quantify the concurrent mechanical changes occurring in the films. Furthermore, in contrast to these three examples, the work presented here utilizes a nanoparticle-based assembly, as redox-active Prussian Blue nanoparticles serve as an integral component of a polymer nanocomposite. (Srivastava and Kotov recently reviewed the field of LbL-assembled nanocomposites,[21] though to our knowledge previous LbL nanocomposite systems have not been investigated for reversible swelling properties.) The advantages in using a redox-active nanoparticle include the potential to manipulate particle loading[22] at or near a percolation threshold, thus yielding more dramatic shifts in electrochemical and mechanical properties, the ability to achieve the multiple redox states exhibited by inorganic materials, and the ability to manipulate surface charge and thus directly impact electrostatics within the film with the accompanying redox behavior, independent of a polyelectrolyte conjugate. These properties make this system interesting as a potential mechanomutable material for which stiffness can be altered significantly with a readily controlled external stimulus.

Prussian Blue (PB), or iron(II) hexacyanoferrate(III), is the first known, mixed valence transition metal complex. Researchers have used PB for a wide range of applications including electrochromic devices,[23,24] glucose sensors,[25,26] and molecular magnets.[27−29] Our group recently utilized Prussian Blue nanoparticles (PB) for an electroactive controlled release coating.[30] When PB is synthesized in its "soluble" form, potassium ions dissociate in aqueous solution, resulting in negatively charged surface and interior sites; this dissociation results in an electrostatically stabilized colloidal suspension. In the native PB oxidation state, roughly half of the iron atoms are in the Fe(II) redox state and the remaining are in the Fe(III) redox state.[31] PB can be electrochemically reduced to Prussian White (PW) or oxidized to Prussian Yellow (PX) (Figure 1a). The PW state has a charge of −2 per unit cell, the PB state has a charge of −1 per unit cell, and the PX state is neutral. This charge shifting capability of PB makes it a very interesting material to study, particularly as a part of composites where altering PB charge can alter properties of the composite as a whole. In previous work, we have shown that oxidizing Prussian Blue nanoparticles can lead to sufficient loss of charge to yield film dissolution and controlled release in LbL thin films.[23,30]

Here we characterize the electrochemically controlled swelling and mechanical behavior of electroactive LbL thin films containing Prussian Blue nanoparticles as the polyanion and linear polyethyleneimine (LPEI) as the polycation. Specifically, we apply −0.2 V (*vs* Ag/AgCl) to reduce the particles from the PB state to the PW state and +0.6 V to oxidize the particles back to the PB state. This negative voltage level is sufficient to fully reduce the PB nanoparticles, and this positive voltage level is sufficient to fully reoxidize the PB without inducing dissolution that can occur at even higher voltages.[23] Upon electrochemical reduction, the negative charge on the particle surface and interior is doubled as estimated from the valence of the two redox states. In response to the excess negative charge created in the film, cations and water from the electrolyte solution enter the film to maintain electroneutrality (Figure 1b). We have investigated the swelling phenomenon using spectroscopic ellipsometry and electrochemical atomic force microscopy (EC-AFM). Nanoindentation and an electrochemical quartz crystal microbalance with dissipation monitoring (EQCM-D) were used to measure the mechanical properties of films in the oxidized and reduced states. To our knowledge, this is the first direct observation of mechanical property manipulation carried out in an electrochemical cell with a redox-active thin film. We believe that electrochemical control over the swelling and mechanical behavior of polymer nanocomposites could be optimized to have important implications for active manipulation of cell behavior on surfaces, as well as responsive coatings for nanoscale devices in general.

**(a)**

| Prussian White | $Fe^{II}[Fe^{II}(CN)_6]^{2-}$ |
| --- | --- |
| | ox. ↓↑ red. |
| Prussian Blue | $Fe^{III}[Fe^{II}(CN)_6]^{1-}$ |
| | ox. ↓↑ red. |
| Prussian Yellow | $Fe^{III}[Fe^{III}(CN)_6]^{0}$ |

**(b)**



**Figure 1.** (a) Redox states of Prussian Blue. (b) Schematic of an (LPEI/PB)$_{30}$ film swelling under the influence of an electric potential. Water molecules and positive charges on the polymer are omitted for clarity. The degree of swelling represented in the figure is exaggerated for the reader's convenience.
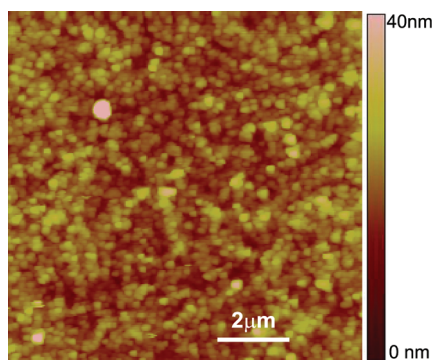
**Figure 2. AFM height image of an (LPEI/PB)$_{30}$ film surface assembled on ITO glass, acquired *via* contact-mode imaging in an aqueous 0.1 M potassium hydrogen phthalate solution; rms roughness is 3.48 ± 0.16 nm.**

## RESULTS AND DISCUSSION

Synthesis of Prussian Blue (PB) nanoparticles, as reported by Delongchamp and Hammond, gives an electrostatically stabilized suspension of negatively charged nanoparticles with a median diameter of 4−5 nm as measured by transmission electron microscopy.[23] Layer-by layer assembly of the PB nanoparticles with linear polyethyleneimine was also characterized previously by our group.[23] This system exhibits linear growth with an average thickness of ~4.1 nm/bilayer in the dry state both on an indium tin oxide (ITO)-coated glass substrate and a gold (Au)-coated silicon substrate. The volume fraction of PB in the films (dry state) is 0.68, calculated from film thickness and Faradaic charge uptake.[23] An approximation of the interparticle distance indicates that the particles are interlocking (see Methods). The root-mean-squared (rms) surface roughness of the films assembled on ITO glass, as calculated from AFM height images, was 3.48 ± 0.16 nm, comparable to the PB nanoparticle diameter (Figure 2).

Passive swelling of (LPEI/PB)$_{30}$ films on Au-coated silicon was measured with spectroscopic ellipsometry (see Methods and Supporting Information for full characterization). We define passive swelling as swelling of a film from the dry state to the hydrated state, in the absence of an applied potential. A typical (LPEI/PB)$_{30}$ film had a dry thickness of ~100 nm, which agreed well with thickness measured by profilometry (data not shown). To measure the time scale of passive swelling, an (LPEI/PB)$_{30}$ film was immersed in a potassium hydrogen phthalate (KHPh) electrolyte solution at pH 4.0 for 1 h. A typical (LPEI/PB)$_{30}$ film swelled by ~12% of its initial dry thickness immediately upon immersion in the electrolyte. Over the course of an hour, the film thickness increased to a final degree of swelling (with respect to the initial dry state) of ~17% (Figure 3a). An identical film allowed to swell passively in electrolyte over 2 days reached a final degree of swelling of 30%. It should be noted that the degree of passive swelling varies depending on the ambient humidity because the "dry" film is equilibrated with vapor in the air.[15] The effect of
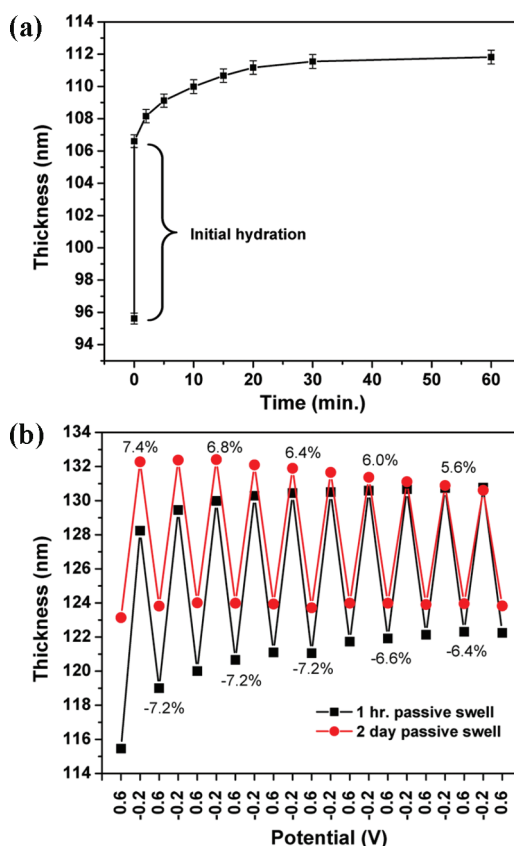


**Figure 3. (a) Passive swelling of an (LPEI/PB)$_{30}$ film in a 0.1 M KHPh electrolyte solution over 1 h. All of the error bars represent 95% confidence intervals based on the ellipsometry model fit. (b) Active swelling of two (LPEI/PB)$_{30}$ films subjected to 10 redox cycles. Error bars representing 95% confidence intervals based on the ellipsometry model fit are approximately the size of the data points. Selected swelling percentage values (calculated relative to thickness in the preceding redox state) are next to the corresponding data points; negative values represent shrinking.**

ionic strength of the electrolyte on degree of passive swelling was also investigated. Identical (LPEI/PB)$_{30}$ films were swollen passively overnight in 1, 10, and 100 mM KHPh solutions each adjusted to pH 4.0 exactly. The films exhibited degrees of swelling of 21.4 ± 1.7, 24.7 ± 0.6, and 26.8 ± 2.2%, respectively, showing that a greater degree of passive swelling resulted for higher ionic strength. In contrast to covalently cross-linked polyelectrolyte hydrogels, this trend is expected for electrostatically assembled layer-by-layer films because mobile ions can compete with the polycation−polyanion linkages in the film. Breakage of some of the cohesive ionic cross-links in the film then results in loosening of the network and additional swelling.[32]

Active swelling of (LPEI/PB)$_{30}$ films on Au-coated silicon was first measured with spectroscopic ellipsometry. We define active swelling as swelling of a hydrated film under the influence of an applied electric potential. Film thicknesses were determined for films subjected to −0.2 V (reduced or PW state) and +0.6 V (oxidized or PB state), alternately. Ellipsometry measurements are

complicated by the fact that the film optical constants differ substantially at the two applied potentials. In the PB state, there was a large absorbance peak centered at ~730−740 nm (1.68 eV) stemming from intervalence charge transfer, while in the PW state, there was a much smaller absorbance peak centered at ~850 nm (1.45 eV). The model and experimental ellipsometric parameter ($\psi$ and $\Delta$) values for an (LPEI/PB)$_{30}$ film at +0.6 and −0.2 V, along with the model fit results, can be found in the Supporting Information (Figure S1). At both applied potentials, we observe excellent agreement between our ellipsometric model fit and the data. Measurements were taken after 2 min at each specified potential. Two minutes were sufficient for the film to attain a stable thickness following redox-induced swelling. Using spectroscopic ellipsometry, a dynamic scan protocol was employed to take measurements every 10 ms while the film underwent electrochemical switching. This experiment revealed that active film swelling is completed within approximately 100 ms, following the application of −0.2 V (Figure S2 in Supporting Information). Figure 3b shows the thickness evolution of two (LPEI/PB)$_{30}$ films submitted to 10 reduction/oxidation cycles, as measured *via* spectroscopic ellipsometry. We observed swelling and shrinking on the order of 5−10% of initial film thickness upon redox, with an average of 6.2 ± 0.6% for the film swollen passively for 2 days (Figure 3b). For the film swollen passively in solution for 1 h, the swelling was not completely reversible in the time scale of our experiment. Specifically, the degree of swelling decreased slightly with successive redox cycles, and film thickness increases, as the film continues to equilibrate with the electrolyte. For the film swollen passively in solution for 2 days, swelling was much more reversible, although there is a slight decrease in degree of swelling after the first few cycles. This cycle-dependent decrease in swelling may be attributable to desorption of a small number of nanoparticles from the film upon early redox cycles or to diffusion of polymers and nanoparticles within the film that change the swellability of the film over time.

Electrochemical AFM (EC-AFM) was used as a complementary technique to directly investigate electrochemically triggered (active) swelling *in situ*. EC-AFM integrates a potentiostat with AFM, allowing simultaneous application of an electric potential and AFM surface measurements. (LPEI/PB)$_{30}$ films assembled on ITO glass were allowed to equilibrate with the electrolyte, an electric potential was then applied to reduce or oxidize the film, and 2 min was allowed to elapse before thickness measurements were carried out. In agreement with spectroscopic ellipsometry, when films were allowed to swell passively for only 30 min, a gradual increase in film thickness was observed with successive redox cycles (data not shown), indicating that the film was not completely equilibrated with the electrolyte in that time scale. When films were allowed to swell pas-
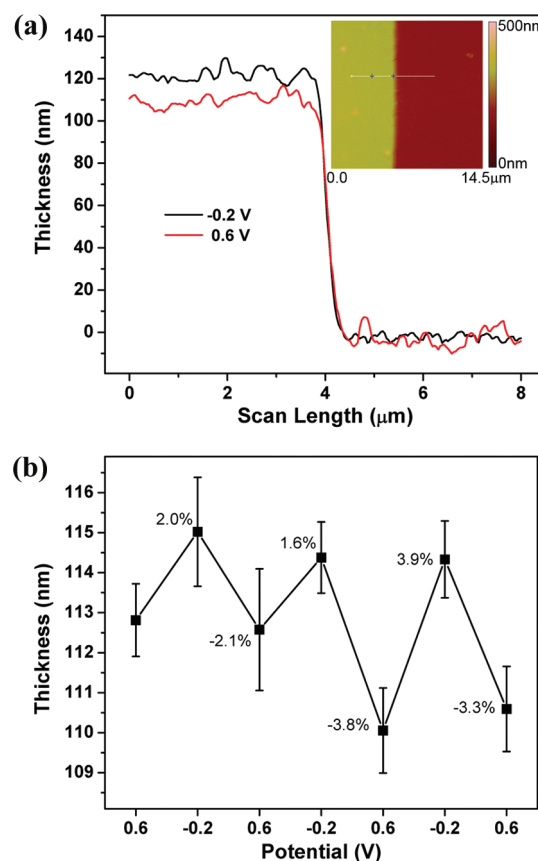


**Figure 4.** (a) Surface profile of an (LPEI/PB)$_{30}$ film measured with EC-AFM at applied potentials of −0.2 and +0.6 V. The inset shows a height image of the film/substrate boundary with a demarcation denoting the location of the surface profile measurement. (b) Evolution of film thickness with successive potential cycling. The error bars represent the standard deviation from $n = 5$ measurements taken at different locations on the film. Swelling percentage values (calculated relative to thickness in the preceding redox state) are next to the data points; negative values represent shrinking.

sively for 2 days, we observed reversible swelling with a more stable baseline film thickness, also in agreement with spectroscopic ellipsometry (Figure 4b). EC-AFM indicates that (LPEI/PB)$_{30}$ films swell and shrink by 2−4% (with an average of 2.8 ± 1.0%) of initial, hydrated film thickness when the PB is electrochemically reduced and oxidized, respectively (Figure 4), compared to the 6.2 ± 0.6% swelling observed with spectroscopic ellipsometry (Figure 3b). The results from spectroscopic ellipsometry and EC-AFM measurements agree well qualitatively, showing that the films swell when reduced and shrink when oxidized, and that swelling is reversible. The large errors in the EC-AFM measurements result from the fact that film surface roughness is on the same order of magnitude as height changes associated with reversible swelling. Furthermore, the EC-AFM likely underestimates the degree of swelling since the AFM tip in contact mode presses on the film surface (average imaging force = 0.4 nN), which can lead to film compression.

It is reasonably anticipated that the (LPEI/PB)$_{30}$ films would swell upon reduction and shrink upon oxidation. When PB is fully reduced to PW, all of the Fe(III) centers are switched to the Fe(II) oxidation state, and the negative charge on each unit cell is theoretically doubled. To maintain electroneutrality, potassium ions (and solvating water molecules) enter the film. The excess of potassium ions in the film relative to the surrounding electrolyte will generate an osmotic pressure, bringing additional water into the film. Film swelling ceases when the elastic forces in the film are balanced by osmotic pressure forces. The forced swelling of redox-active thin films to maintain electroneutrality has been observed by a number of other authors.[33−36] The phenomenon of a continual increase in film thickness with successive redox cycles was also observed by Grumelli *et al.* for the case of (PAH-Os/PSS) multilayer films.[34] They attribute this occurrence to "break in" of the electrolyte, where polycation−polyanion electrostatic interactions are broken by mobile cations and anions, resulting in irreversible solvent uptake and partially "extrinsic" charge compensation in the film. Similarly, we suspect that an influx of ions induced by PB reduction can break ionic cross-links in the film leading to further reduction in the mechanical stiffness of the composite material, beyond that which would be caused by swelling alone.

The mechanical behavior of the (LPEI/PB) composite films on ITO glass, in response to electrochemical redox of PB within the films, was analyzed with instrumented nanoindentation in aqueous conditions and with EQCM-D. Instrumented, spherical nanoindentation enabled determination of the effective Young's elastic modulus of the composite films, fully immersed in 0.1 M KHPh at room temperature (see Methods). Figure 5a shows typical load-depth responses for an (LPEI/PB)$_{50}$ film in the oxidized state (+0.6 V) and the reduced state (−0.2 V). Clearly, the film is more compliant in the reduced state, consistent with an increase in hydration upon film swelling. An effective Young's elastic modulus, $E_i$, was determined from these indentation responses of the hydrated composite film, correcting for the finite thickness of each film and the stiffness of the underlying ITO glass substrate (see Methods). Figure 5b shows $E_i$ of a film subjected to two redox cycles. After allowing the film to swell in the electrolyte solution for 2 h, $E_i$ was measured to be 3.40 ± 1.03 GPa. Subsequent electrochemical reduction of the film reduced $E_i$ further to 1.75 ± 0.26 GPa, a decrease of nearly 50%. Upon reoxidation of the film, $E_i$ returned to 3.54 ± 0.64 GPa; subsequent electrochemical reduction then reduced $E_i$ to 2.14 ± 0.6 GPa. Measurements at each potential were taken over the course of 1 h and exhibited excellent repeatability, attesting to the stability of the films and the reversibility of the switching. As expected, the indentation elastic modulus of the film in the absence of an applied potential (*i.e.*, at the open circuit potential) is
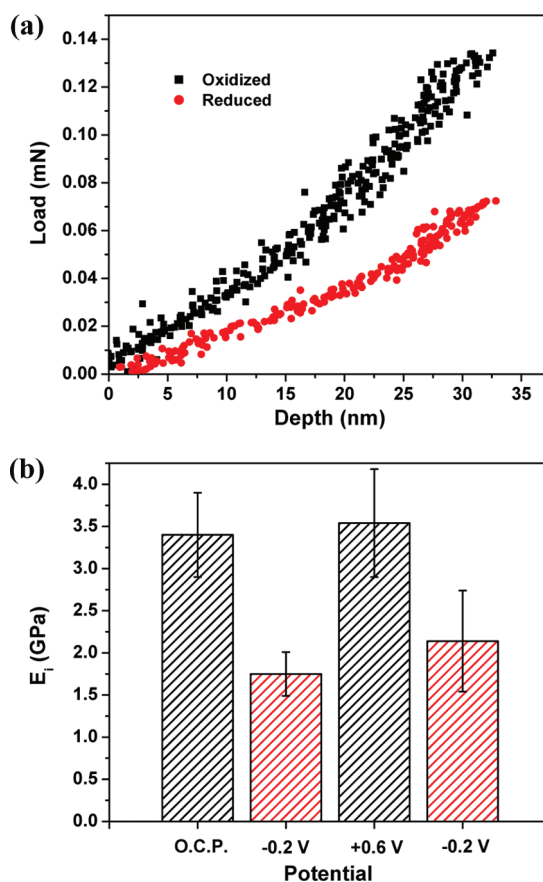


**Figure 5. Instrumented nanoindentation results for an (LPEI/PB)$_{50}$ film immersed in aqueous 0.1 M KHPh. (a) Loading portion of the load-depth response for a film in the oxidized (black, +0.6 V) and reduced (red, −0.2 V) state. (b) Effective Young's elastic moduli $E_i$ of the film subjected to two redox cycles, corrected for finite thickness as described in Methods. OCP stands for open circuit potential. Error bars represent the standard deviation from $n = 6$ measurements at different locations on the film for each condition.**

equal to that at +0.6 V since the PB redox state is largely unchanged between the open circuit potential (typically +0.3 to +0.4 V) and +0.6 V (Figure 7). For refer-
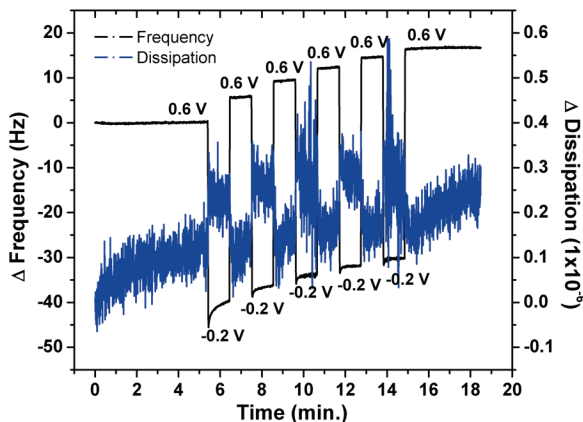


**Figure 6. Change in frequency and dissipation (13th overtone) of a Au-coated QCM crystal modified with an (LPEI/PB)$_{30}$ film upon alternate application of −0.2 and +0.6 V (*vs* Ag/AgCl). Signal-to-noise of dissipation at the lower frequency overtones was insufficient to identify changes upon voltage switching.**
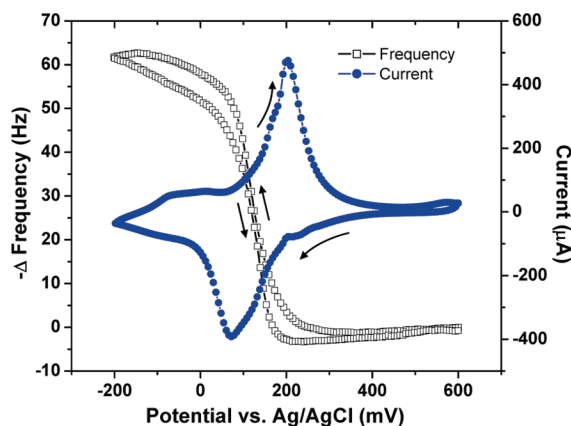
**Figure 7.** Overlay of a cyclic voltammogram and EQCM frequency data (3rd overtone) for an (LPEI/PB)$_{30}$ film. Scan rate is 10 mV/s. The inflection in frequency (mass change) corresponds with the potential of the Prussian Blue−Prussian White redox couple.

ence, an (LPEI/PB)$_{50}$ film in the dry state exhibited $E_i$ = 6.92 ± 1.03 GPa (data not shown). Note that, although these elastic moduli exceed expected Young's elastic moduli of fully hydrated polyelectrolyte-based hydrogels,[7] these (LPEI/PB)$_{50}$ nanocomposites comprise 68 vol % of the stiff, inorganic crystalline PB phase.

As expected, the elastic modulus of the film decreases upon immersion in the electrolyte solution and then decreases further upon electrochemical reduction of the film. Specifically, a *ca.* 50% reduction in $E_i$ accompanies swelling of the hydrated film upon redox (*ca.* 5−10% as measured *via* spectroscopic ellipsometry in Figure 3b and 2−4% as measured *via* EC-AFM in Figure 4b). During swelling, the incoming water and ions serve as plasticizers to reduce cohesive interactions in the film. Furthermore, incoming ions can break ionic cross-links in the film, thereby giving polymer segments additional degrees of translational freedom and rendering the film less stiff. The extent of decrease in the elastic modulus as a function of swelling observed here is similar in magnitude to that observed for other LbL films in the Schlenoff group[16,32] and the Van Vliet and Rubner groups[37,38] (see Supporting Information for a quantitative comparison). Jaber and Schlenoff recently showed that the elastic modulus of other LbL films can be decreased substantially (for relatively small degrees of swelling)[32] by increasing the ionic strength of the surrounding solution, which decreases the ionic cross-link density in the film.[16] Here we maintain the ionic strength of the electrolyte constant, but instead induce increased ionic strength within the film by exploiting PB redox chemistry.

To access the shear and viscous components of mechanical behavior in these films, EQCM-D was employed. In addition to following frequency changes of the quartz crystal oscillator, EQCM-D records the dissipation or damping of the crystal oscillations when the driving voltage is shut off. A change in dissipation can be related to the shear (storage) elastic modulus and shear viscosity of a viscoelastic film adhered to the crystal.[39] When (LPEI/PB)$_{30}$ films assembled on Au-coated quartz were switched from a potential of +0.6 to −0.2 V (*vs* Ag/AgCl), the resonant frequency of the quartz crystal decreased, and the oscillation dissipation of the crystal increased (Figure 6). These results indicate mass uptake by the film and a qualitative increase in the viscous component of a viscoelastic response, respectively. However, the change in dissipation relative to the change in frequency was too small to allow for viscoelastic modeling of the film with the Voigt model. Furthermore, the frequency responses of the third through thirteenth overtones (normalized by overtone number) overlapped exactly, indicating the rigidity of the film and applicability of the Sauerbrey equation.[40] Therefore, despite changes in dissipation, we were limited to only qualitative conclusions regarding viscoelasticity of the film.

As described earlier, the proposed trigger for swelling of the (LPEI/PB) nanocomposite is the electrochemical reduction of PB. To discern whether this is the case, EQCM was used to measure mass uptake at intermediate applied potentials between the oxidized and reduced film states (Figure 7). There is minimal hysteresis, and the inflection in mass uptake, which occurs at 0.127 V (reduction cycle) and 0.134 V (oxidation cycle), corresponds well with the measured half-wave potential ($E_{1/2}$) of the PB−PW redox couple (0.138 V). This result suggests that electrochemical reduction of PB is responsible for the film swelling phenomenon, as opposed to other possible mechanisms such as double-layer charging effects. As the charge on each PB unit cell is increased, swelling occurs *via* the influx of counterions to maintain electroneutrality in the film, along with osmotic-driven flow of water into the film. This mechanism is similar to that proposed by other authors for redox-active LbL films.[18] The trend of decreased stiffness with increased charge in the film is clearly dependent on the fact that ionic cross-links hold the film together. The opposite trend is observed in certain biological tissues, such as cartilage, where increased effective charge density (attained by minimizing shielding) results in stronger electrostatic repulsions between charged groups, which stiffen the material.[41]

## CONCLUSIONS

The electrochemically triggered swelling behavior and elastic modulus reduction of a polymer nanocomposite film containing Prussian Blue nanoparticles and linear polyethyleneimine has been described. Reduction of the Prussian Blue (PB) in the films to Prussian White doubles the negative charge on the nanoparticle surface and interior. An influx of ions and water from the surrounding solu-

tion occurs to maintain electroneutrality in the film and results in film swelling and decreased mechanical stiffness of the composite. Subsequent oxidation back to the PB state causes the film to deswell and return to its original stiffness. The swelling phenomenon, characterized using spectroscopic ellipsometry and EC-AFM, is concurrent with a reduction in the film elastic modulus as measured *via* instrumented nanoindentation in aqueous conditions.

The system described here is distinct from existing electrochemically active multilayer systems in several ways. The electroactive species in our films is an integral and structural component of the film, thus requiring only that the film be immersed in an electrolyte solution containing potassium ions for PB switching. On the other hand, the PB in our system exists as nanoparticles and, as such, the polyethyleneimine–Prussian Blue system is a polymer nanocomposite that can exhibit percolative mechanical behavior. While the stiffness of typical polymer-based layer-by-layer assemblies can be changed by an influx of water and ions, the stiffness of a polymer nanocomposite LbL assembly could be further affected by interactions between adjacent filler particles. We posit that the ability to electrochemically modulate the thickness of a polymer-based nanocomposite could lead to interesting control over the mechanical properties of the composite as the particle percolation threshold is approached. We are currently designing electroactive composites at the mechanical percolation threshold, which is the critical fraction of filler above which the filler particles interact with each other with the potential to significantly stiffen the composite in the initial redox state. Assembly of composite films at or near the percolation threshold could facilitate

dramatic mechanical and swelling changes upon redox, as the influx of ions and water could disrupt the percolation network and thus decrease the composite stiffness.

A future system that could be engineered to achieve rapid, dramatic mechanical changes with only slight changes in degree of swelling could be applied to the control of cellular behavior on surfaces. For example, on/off switching of cell adhesion could allow cells to be guided to particular locations within microfluidic devices or cells could be triggered to differentiate for tissue engineering applications or fundamental studies. The system reported here, however, is likely too stiff to modulate cellular behavior. Previous reports on the tunability of cellular adhesion, locomotion, and differentiation with substrata stiffness utilize substrates with elastic modulus values in the range of 1 kPa up to 100 MPa and generally consider 1–2 orders of magnitude changes in elastic moduli.[6,7,12,42] Therefore, the stiffness and mutability of a future electroactive mechanomutable surface must be engineered to access most cell-based applications. Nonetheless, we have introduced a new framework for electrically modulating the stiffness of a composite. Further, the fact that our system is a composite opens up the possibility of investigating disruptable percolative networks in which interactions between nanoparticles are turned on and off with an electrochemical trigger. This area represents a new direction in biomimicry since a number of marine organisms can rapidly alter their stiffness through percolative behavior. This work can thus serve as a starting point for further studies on mechanomutable coatings with potential future applications in micro- and nanoscale devices.

## METHODS

**Materials.** Linear polyethyleneimine (LPEI) ($M_n = 25\,000$) was purchased from Polysciences. Iron(II) chloride tetrahydrate, potassium ferricyanide, potassium hydrogen phthalate (KHPh), and 3-mercapto-1-propanesulfonic acid (MPS) were purchased from Sigma Aldrich. Potassium chloride was purchased from Mallinckrodt Baker. All chemicals were used as received. Gold-coated silicon wafers (AU.1000.SL1) consisting of a 1000 Å layer of gold with a 50 Å titanium adhesion layer were purchased from Platypus Technologies, LLC. Gold-coated QCM crystals (QSX 301) consisting of a 1000 Å layer of gold with a 50 Å chromium adhesion layer were purchased from Q-Sense, Inc. Indium tin oxide (ITO)-coated glass slides (CD-50IN-CUV) were purchased from Delta Technologies, Limited.

**Synthesis of Prussian Blue Nanoparticles.** Synthesis of PB nanoparticles was carried out as described previously.[23] Briefly, 50 mL of aqueous 10 mM $FeCl_2 \cdot 4H_2O$ was added dropwise to an equivalent volume of aqueous 50 mM $K_3[Fe(CN)_6]$ and 50 mM KCl with vigorous stirring. The dark green mixture was immediately submitted to dialysis against a regenerated cellulose membrane with a 3500 Da molecular weight cutoff to remove excess $K_3[Fe(CN)_6]$ and KCl. The resulting blue nanoparticle suspension was adjusted to pH 4 with potassium hydrogen phthalate (KHPh) (final concentration of 1 mM) and hydrochloric acid.

**Assembly of LPEI/PB Films.** Films were assembled on gold-coated silicon wafers, gold-coated quartz crystals, or ITO-coated glass slides. The gold-coated silicon was cleaned by immersion in gold cleaning solution (Sigma Aldrich) for 1 min, rinsed copiously with deionized water, and then immersed in an aqueous solution of 20 mM 3-mercapto-1-propanesulfonic acid (MPS) and 16 mM sulfuric acid for 30 min to render the surface negatively charged. Thereafter, the substrates were again rinsed thoroughly with deionized water and used for subsequent layer-by-layer assembly. The gold-coated quartz crystals were cleaned by UV/ozone treatment for 10 min, immersion in a $H_2O/H_2O_2/NH_3$ (5:1:1) solution at 75 °C for 5 min followed by a thorough deionized water rinse, and a second UV/ozone treatment for 10 min. Following the cleaning, the crystals were immediately immersed in the MPS solution described above for 30 min. ITO-coated slides were cleaned by sonication in a 4% solution of Micro-90 detergent for 15 min, following by two 15 min sonication cycles in deionized water. LPEI solutions were prepared in deionized water at a concentration of 10 mM based on the polymer repeat unit. The solution pH was adjusted to the desired value with HCl and NaOH. $(LPEI/PB)_n$ films, where $n$ denotes the number of bilayers, were assembled by dip coating using an automated Zeiss HMS series programmable slide stainer. Briefly, substrates were immersed in an LPEI solution for 10 min followed by three separate deionized water rinse baths (adjusted to pH 4 with KHPh and HCl) for a total of 3 min. Next, the substrates were immersed

in a PB solution for 10 min followed by the same cascade rinse cycle. Gold-coated silicon was used for spectroscopic ellipsometry, gold-coated quartz was used for EQCM-D, and ITO glass was used for EC-AFM. Note that the different substrates did not have an appreciable effect on film thickness, roughness, or the linear growth profile. Slight differences in initial film thickness from sample to sample can be attributed to slight variations in pH of the solutions used for the deposition process. Interparticle distance in the films (in the hydrated state) was approximated assuming spherical particles with a uniform size distribution and dispersion using the equation presented by Hong et al.[43] We obtained a negative value, implying that the particles are interlocking.

**Atomic Force Microscopy (AFM).** AFM imaging of $(LPEI/PB)_{30}$ films on ITO glass substrates was used for visualization of surface morphology and calculation of the root-mean-squared (rms) surface roughness of the films. Measurements were made using a Nanoscope IV (IV/IIIa emulation controller) multimode scanning probe microscope (Digital Instruments/Veeco Metrology Group, Santa Barbara, CA) in contact mode. Films were measured in their hydrated state using a fluid cell (Veeco ECFC) loaded with ca. 20−50 μL of 0.1 M potassium hydrogen phthalate (KHPh) electrolyte solution at pH 4.0. Films were allowed to equilibrate with the solution for 30 min before measurement. A silicon nitride $(Si_3N_4,$ SNL, Veeco Probes, Santa Barbara, CA) cantilever with a nominal spring constant of 0.06 N/m carrying a tip with a nominal diameter of 2 nm was attached to the fluid cell with a gold spring. The rms roughness was calculated from five 3 μm × 3 μm height images using Veeco NanoScope v.614r1 software. Tip shape deconvolution of image height and roughness calculations was carried out using SPIP (Scanning Probe Image Processor v4.8.4) software.

**Spectroscopic Ellipsometry.** Spectroscopic ellipsometry analysis of $(LPEI/PB)_{30}$ films on gold-coated silicon substrates was carried out using a J.A. Woollam M-2000 instrument. Data were fit using J.A. Woollam WVASE32 software. In situ measurements were conducted through a custom-made quartz cell with 70° windows (Hellma USA, Inc.). Spectroscopic ellipsometry measures the change in polarization state of light reflected from a surface. Two ellipsometric parameters, ψ and Δ, representing the change in amplitude and phase of the reflected light, respectively, are collected at a number of wavelengths; ψ and Δ are related to the thickness and optical constants of the sample. Briefly, to determine film thickness with spectroscopic ellipsometry, we used a single Gaussian oscillator to model the film absorbance from 620 to 900 nm. See the Supporting Information for further details on modeling of spectroscopic ellipsometry data. To simultaneously apply a voltage to a film while characterizing the film with spectroscopic ellipsometry, a three-electrode electrochemical cell was set up in the quartz cell with a Ag/AgCl reference electrode (Bioanalytical Systems, Inc.), a Pt coil counter electrode, and a gold-coated silicon wafer modified with a $(LPEI/PB)_n$ film as the working electrode. The electrolyte was a 0.1 M KHPh solution with pH 4.0. An AutoLab PGSTAT100 potentiostat was used for electrochemical measurements. Two minutes was allowed to elapse at each applied potential, before taking a measurement. A dynamic scan protocol in the WVASE32 software package with acquisition time of 10 ms was used to capture the kinetics of the redox-induced swelling process.

**Electrochemical Atomic Force Microscopy (EC-AFM).** EC-AFM of $(LPEI/PB)_{30}$ films on ITO glass substrates was performed using a Nanoscope IV (IV/IIIa emulation controller) multimode scanning probe microscope (Digital Instruments/Veeco Metrology Group, Santa Barbara, CA) in contact mode with an integrated multimode EC basic potentiostat. (Note that this platform does not support tapping mode AFM.) The film sample was attached to the magnetic sample holder using double-sided tape and was placed on the E-type piezo scanner. Electrical contact between the ITO and the sample puck was made with silver paste. A three-electrode-type glass EC fluid cell was used for the contact mode measurements. The cell volume was ca. 20−50 μL, and 0.1 M KHPh with pH 4.0 was used as the electrolyte. A silicon nitride $(Si_3N_4,$ SNL, Veeco Probes, Santa Barbara, CA) cantilever with a

nominal spring constant of 0.06 N/m carrying a tip with a nominal diameter of 2 nm was attached to the fluid cell with a gold spring. A silver wire and a platinum wire were used as a pseudoreference electrode and counter electrode, respectively. An electric potential was applied using the chronoamperometry function, and 2 min was allowed to elapse before surface profiles were captured. Thickness values of the films were calculated as follows. A box was drawn on a flat area of the substrate, and a first-order plane fit was applied. A 10 μm scan length was acquired under a nominal contact load of 0.4 nN, traversing the edge of the film, and the average heights of the film and substrate were determined by simple averaging of the individual data points. The same locations at the film/substrate interface were line-scanned before and after redox.

**Nanoindentation.** Nanoindentation on $(LPEI/PB)_{50}$ films on ITO glass was conducted by a pendulum-based instrumented nanoindenter (NanoTest, Micro Materials Ltd.) with a force resolution of 1 μN and a displacement resolution of 0.1 nm. Films assembled on ITO-coated glass were adhered to an aluminum support with a thin layer of cyanoacrylate, and all of the experiments were conducted with the sample fully immersed in 0.1 M KHPh, using a modified platform for in situ liquid experiments.[44] An electrochemical cell was set up within the liquid cell with the film as the working electrode, a Pt wire as the counter electrode, and a silver wire as a pseudoreference electrode. The potential was controlled with an EG&G 263A potentiostat/galvanostat. Samples were indented with a spherical ruby indenter of radius $R = 5$ μm, both in the oxidized and reduced states of the film ($n = 6$ locations for each condition), with loading, dwell, and unloading times of 10, 10, and 2 s, respectively. A maximum depth of 40 nm was chosen to induce comparable, low strains on all samples (∼10%), and the corresponding maximum loads ranged between 80 and 200 μN. Film Young's elastic modulus inferred from indentation, $E_i$, was calculated through a finite-thickness correction of Hertzian elastic contact, using the model of Dimitriadis et al.,[45] in order to account for mechanical contributions from the underlying stiff ITO glass substrate for the measured film thickness of 224 ± 13 nm (as determined via profilometry). $E_i$ of the film is related directly to the Young's elastic modulus $E$ that is typically measured via uniaxial loading of macroscopic materials and is theoretically equivalent to $E$ for linear elastic materials. Thicker films (50 bilayers instead of 30 bilayers) were used to improve the accuracy of nanoindentation by allowing for a deeper penetration depth. From spectroscopic ellipsometry analysis, 50-bilayer films were found to swell to the same degree as 30-bilayer films (data not shown).

**Electrochemical Quartz Crystal Microbalance with Dissipation (EQCM-D).** EQCM-D analysis of $(LPEI/PB)_{30}$ films on gold-coated quartz was carried out using a Q-Sense E1 system along with the electrochemistry module (QEM 401). Frequency changes are directly proportional to mass changes according to the Sauerbrey equation.[46] $(LPEI/PB)_{30}$ films were assembled on gold-coated QCM crystals (Q-Sense QSX 301) as described above, and the film was removed from the backside of the crystals using a cotton swab soaked in 1 M NaOH, following by a deionized water rinse. The QCM chamber served as a three-electrode electrochemical cell with a Ag/AgCl reference electrode (Cypress Systems), a built-in Pt counter electrode, and the Au-coated QCM crystal modified with an $(LPEI/PB)_{30}$ film as the working electrode. The electrolyte was a 0.1 M KHPh solution with pH 4.0. A VoltaLab 21 potentiostat was used for electrochemical measurements.

*Supporting Information Available:* Spectroscopic ellipsometry modeling strategy and fit results for (LPEI/PB)$_{30}$ films in the oxidized and reduced states, dynamic spectroscopic ellipsometry scan results, and additional mechanical analysis. This material is available free of charge *via* the Internet at http://pubs.acs.org.

## REFERENCES AND NOTES

1. Ahn, S. K.; Kasi, R. M.; Kim, S. C.; Sharma, N.; Zhou, Y. X. Stimuli-Responsive Polymer Gels. *Soft Matter* **2008**, *4*, 1151–1157.
2. Ganta, S.; Devalapally, H.; Shahiwala, A.; Amiji, M. A Review of Stimuli-Responsive Nanocarriers for Drug and Gene Delivery. *J. Controlled Release* **2008**, *126*, 187–204.
3. Mano, J. F. Stimuli-Responsive Polymeric Systems for Biomedical Applications. *Adv. Eng. Mater.* **2008**, *10*, 515–527.
4. Mendes, P. M. Stimuli-Responsive Surfaces for Bio-Applications. *Chem. Soc. Rev.* **2008**, *37*, 2512–2529.
5. Nelson, A. Stimuli-Responsive Polymers—Engineering Interactions. *Nat. Mater.* **2008**, *7*, 523–525.
6. Discher, D. E.; Janmey, P.; Wang, Y. L. Tissue Cells Feel and Respond to the Stiffness of Their Substrate. *Science* **2005**, *310*, 1139–1143.
7. Thompson, M. T.; Berg, M. C.; Tobias, I. S.; Rubner, M. F.; Van Vliet, K. J. Tuning Compliance of Nanoscale Polyelectrolyte Multilayers to Modulate Cell Adhesion. *Biomaterials* **2005**, *26*, 6836–6845.
8. Capadona, J. R.; Shanmuganathan, K.; Tyler, D. J.; Rowan, S. J.; Weder, C. Stimuli-Responsive Polymer Nanocomposites Inspired by the Sea Cucumber Dermis. *Science* **2008**, *319*, 1370–1374.
9. Favier, V.; Canova, G. R.; Shrivastava, S. C.; Cavaille, J. Y. Mechanical Percolation in Cellulose Whisker Nanocomposites. *Polym. Eng. Sci.* **1997**, *37*, 1732–1739.
10. Flandin, L.; Bidan, G.; Brechet, Y.; Cavaille, J. Y. New Nanocomposite Materials Made of an Insulating Matrix and Conducting Fillers: Processing and Properties. *Polym. Compos.* **2000**, *21*, 165–174.
11. Decher, G. Fuzzy Nanoassemblies: Toward Layered Polymeric Multicomposites. *Science* **1997**, *277*, 1232–1237.
12. Ren, K. F.; Crouzier, T.; Roy, C.; Picart, C. Polyelectrolyte Multilayer Films of Controlled Stiffness Modulate Myoblast Cell Differentiation. *Adv. Funct. Mater.* **2008**, *18*, 1378–1389.
13. Thompson, M. T.; Berg, M. C.; Tobias, I. S.; Lichter, J. A.; Rubner, M. F.; Van Vliet, K. J. Biochemical Functionalization of Polymeric Cell Substrata Can Alter Mechanical Compliance. *Biomacromolecules* **2006**, *7*, 1990–1995.
14. Sukhishvili, S. A. Responsive Polymer Films and Capsules *via* Layer-by-Layer Assembly. *Curr. Opin. Colloid Interface Sci.* **2005**, *10*, 37–44.
15. Nolte, A. J.; Treat, N. D.; Cohen, R. E.; Rubner, M. F. Effect of Relative Humidity on the Young's Modulus of Polyelectrolyte Multilayer Films and Related Nonionic Polymers. *Macromolecules* **2008**, *41*, 5793–5798.
16. Jaber, J. A.; Schlenoff, J. B. Mechanical Properties of Reversibly Cross-Linked Ultrathin Polyelectrolyte Complexes. *J. Am. Chem. Soc.* **2006**, *128*, 2940–2947.
17. Hodak, J.; Etchenique, R.; Calvo, E. J.; Singhal, K.; Bartlett, P. N. Layer-by-Layer Self-Assembly of Glucose Oxidase with a Poly(allylamine)ferrocene Redox Mediator. *Langmuir* **1997**, *13*, 2708–2716.
18. Forzani, E. S.; Perez, M. A.; Teijelo, M. L.; Calvo, E. J. Redox Driven Swelling of Layer-by-Layer Enzyme-Polyelectrolyte Multilayers. *Langmuir* **2002**, *18*, 9867–9873.
19. Ma, Y. J.; Dong, W. F.; Hempenius, M. A.; Möhwald, H.; Vancso, G. J. Redox-Controlled Molecular Permeability of Composite-Wall Microcapsules. *Nat. Mater.* **2006**, *5*, 724–729.
20. Grieshaber, D.; Voros, J.; Zambelli, T.; Ball, V.; Schaaf, P.; Voegel, J. C.; Boulmedais, F. Swelling and Contraction of Ferrocyanide-Containing Polyelectrolyte Multilayers upon Application of an Electric Potential. *Langmuir* **2008**, *24*, 13668–13676.
21. Srivastava, S.; Kotov, N. A. Composite Layer-by-Layer (LBL) Assembly with Inorganic Nanoparticles and Nanowires. *Acc. Chem. Res.* **2008**, *41*, 1831–1841.
22. Particle loading in LbL assemblies can be altered by changing film architecture (*e.g.*, adding extra polymer layers to space apart nanoparticle layers) or by changing film assembly conditions (*e.g.*, deposition time).[21]
23. DeLongchamp, D. M.; Hammond, P. T. High-Contrast Electrochromism and Controllable Dissolution of Assembled Prussian Blue/Polymer Nanocomposites. *Adv. Funct. Mater.* **2004**, *14*, 224–232.
24. Mortimer, R. J. Electrochromic Materials. *Chem. Soc. Rev.* **1997**, *26*, 147–156.
25. Karyakin, A. A.; Gitelmacher, O. V.; Karyakina, E. E. Prussian Blue Based First-Generation Biosensor—A Sensitive Amperometric Electrode for Glucose. *Anal. Chem.* **1995**, *67*, 2419–2423.
26. Zhao, W.; Xu, J. J.; Shi, C. G.; Chen, H. Y. Multilayer Membranes *via* Layer-by-Layer Deposition of Organic Polymer Protected Prussian Blue Nanoparticles and Glucose Oxidase for Glucose Biosensing. *Langmuir* **2005**, *21*, 9630–9634.
27. Jaiswal, A.; Colins, J.; Agricole, B.; Delhaes, P.; Ravaine, S. Layer-by-Layer Self-Assembly of Prussian Blue Colloids. *J. Colloid Interface Sci.* **2003**, *261*, 330–335.
28. Mingotaud, C.; Lafuente, C.; Amiell, J.; Delhaes, P. Ferromagnetic Langmuir—Blodgett Film Based on Prussian Blue. *Langmuir* **1999**, *15*, 289–292.
29. Uemura, T.; Ohba, M.; Kitagawa, S. Size and Surface Effects of Prussian Blue Nanoparticles Protected by Organic Polymers. *Inorg. Chem.* **2004**, *43*, 7339–7345.
30. Wood, K. C.; Zacharia, N. S.; Schmidt, D. J.; Wrightman, S. N.; Andaya, B. J.; Hammond, P. T. Electroactive Controlled Release Thin Films. *Proc. Natl. Acad. Sci. U.S.A.* **2008**, *105*, 2280–2285.
31. Keggin, J. F.; Miles, F. D. Structures and Formulae of the Prussian Blues and Related Compounds. *Nature* **1936**, *137*, 577–578.
32. Dubas, S. T.; Schlenoff, J. B. Swelling and Smoothing of Polyelectrolyte Multilayers by Salt. *Langmuir* **2001**, *17*, 7725–7727.
33. Barbero, C.; Calvo, E. J.; Etchenique, R.; Morales, G. M.; Otero, M. An EQCM Electroacoustic Study of Poly(vinylferrocene) Modified Electrodes in Different Aqueous Electrolytes. *Electrochim. Acta* **2000**, *45*, 3895–3906.
34. Grumelli, D.; Bonazzola, C.; Calvo, E. J. Hydration Cycling in Redox Active LBL Self-Assembled Polyelectrolyte Multilayers. *Electrochem. Commun.* **2006**, *8*, 1353–1357.
35. Hillman, A. R.; Mohamoud, M. A. Ion, Solvent and Polymer Dynamics in Polyaniline Conducting Polymer Films. *Electrochim. Acta* **2006**, *51*, 6018–6024.
36. Tagliazucchi, M.; Grumelli, D.; Calvo, E. J. Nanostructured Modified Electrodes: Role of Ions and Solvent Flux in Redox Active Polyelectrolyte Multilayer Films. *Phys. Chem. Chem. Phys.* **2006**, *8*, 5086–5095.
37. Lichter, J. A.; Thompson, M. T.; Delgadillo, M.; Nishikawa, T.; Rubner, M. F.; Van Vliet, K. J. Substrata Mechanical Stiffness Can Regulate Adhesion of Viable Bacteria. *Biomacromolecules* **2008**, *9*, 1571–1578.
38. Mendelsohn, J. D.; Yang, S. Y.; Hiller, J.; Hochbaum, A. I.; Rubner, M. F. Rational Design of Cytophilic and Cytophobic Polyelectrolyte Multilayer Thin Films. *Biomacromolecules* **2003**, *4*, 96–106.
39. Voinova, M. V.; Rodahl, M.; Jonson, M.; Kasemo, B. Viscoelastic Acoustic Response of Layered Polymer Films at Fluid—Solid Interfaces: Continuum Mechanics Approach. *Phys. Scr.* **1999**, *59*, 391–396.
40. Johannsmann, D. Viscoelastic, Mechanical, and Dielectric Measurements on Complex Samples with the Quartz Crystal Microbalance. *Phys. Chem. Chem. Phys.* **2008**, *10*, 4516–4534.
41. Dean, D.; Han, L.; Ortiz, C.; Grodzinsky, A. J. Nanoscale Conformation and Compressibility of Cartilage Aggrecan

Using Microcontact Printing and Atomic Force Microscopy. *Macromolecules* **2005**, *38*, 4047–4049.

42. Levental, I.; Georges, P. C.; Janmey, P. A. Soft Biological Materials and Their Impact on Cell Function. *Soft Matter* **2007**, *3*, 299–306.

43. Hong, J. I.; Schadler, L. S.; Siegel, R. W.; Martensson, E. Rescaled Electrical Properties of ZnO/Low Density Polyethylene Nanocomposites. *Appl. Phys. Lett.* **2003**, *82*, 1956–1958.

44. Constantinides, G.; Kalcioglu, Z. I.; McFarland, M.; Smith, J. F.; Van Vliet, K. J. Probing Mechanical Properties of Fully Hydrated Gels and Biological Tissues. *J. Biomech.* **2008**, *41*, 3285–3289.

45. Dimitriadis, E. K.; Horkay, F.; Maresca, J.; Kachar, B.; Chadwick, R. S. Determination of Elastic Moduli of Thin Layers of Soft Material Using the Atomic Force Microscope. *Biophys. J.* **2002**, *82*, 2798–2810.

46. Sauerbrey, G. Verwendung von Schwingquarzen zur Wägung dünner Schichten und zur Microwägung. *Z. Phys.* **1959**, *155*, 206–222.